Erschienen in: Europhysics Letters (EPL) ; 74 (2006), 6. - S. 937-943
https://dx.doi.org/10.1209/epl/i2006-10052-6

Stochastic resonance *vs.* resonant activation

C. Schmitt[1], B. Dybiec[2], P. Hänggi[3] and C. Bechinger[1]

[1] *2. Physikalisches Institut, Universität Stuttgart - Pfaffenwaldring 57 70569 Stuttgart, Germany*
[2] *Marian Smoluchowski Institute of Physics and Mark Kac Center for Complex Systems Research, Jagellonian University - ul. Reymonta 4, 30-059 Kraków, Poland*
[3] *Institut für Physik, Universität Augsburg - Universitätsstr. 1 86135 Augsburg, Germany*

PACS. 02.50.Ey – Stochastic processes.
PACS. 82.20.Uv – Stochastic theories of rate constants.
PACS. 82.70.Dd – Colloids.

Abstract. – The phenomenon of stochastic resonance by which it is possible to boost the transduction of information by tuning into noise is experimentally and numerically contrasted with the phenomenon of resonant activation, *i.e.* the occurrence of a minimal, averaged residence time at an optimal time-scale in the presence of barrier modulations. The experimental system consists of a periodically modulated bistable colloidal Brownian dynamics. Interestingly enough, the two phenomena may occur simultaneously in the same system, although typically in quite different parameter regimes.

The application of a suitable dose of noise can significantly enhance the synchronization of a system's response to periodic signals. The most intriguing example for this is stochastic resonance (SR) where the response of a nonlinear system to a periodic signal is optimized by the presence of a certain amount of noise [1]. SR is a generic effect and has been experimentally observed in digital devices and an abundance of physical systems [1–6]. In addition, there emerges continuing evidence suggesting the role of SR for intrinsic use and function in biological systems [7]. Another widely studied phenomenon manifesting the constructive role of noise in physical systems is resonant activation (RA) [8–11]. Here, the cooperative interplay between the barrier modulation process and thermal noise assisting barrier crossing events can cause an enhancement of the reaction kinetics. As such, RA is a generic effect for the barrier crossing dynamics of temporally modulated energy landscapes [8–14].

Despite the apparent similarity of SR and RA, it is important to realize a fundamental difference between the two phenomena: While in SR the constructive role of noise is to optimize and synchronize the actual response when metastable states are periodically modulated [1, 7] the RA phenomenon maximizes the time-averaged escape rate over a time-modulated energy barrier. Therefore, it is expected that a system's response to a periodic signal generally cannot be optimized simultaneously for SR and RA, but is either optimized for the strength of the modulated response (at the expense of the transition rate) or for the optimal, shortest mean

Konstanzer Online-Publikations-System (KOPS)
URL: http://nbn-resolving.de/urn:nbn:de:bsz:352-0-410627

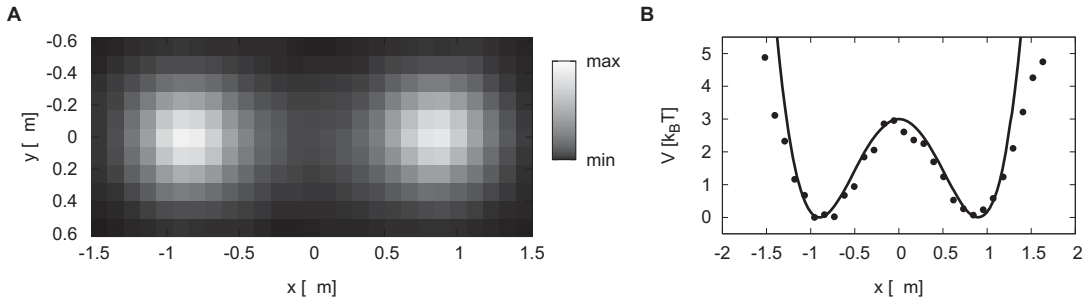

Fig. 1 – A) Two-dimensional probability distribution $P(x, y)$ of a particle's position in the static double-well potential underlying the measurements. B) Cross-section of the potential at $y \approx 0\,\mu$m reconstructed from $P(x, y)$ (symbols) with $V(x)$ used in the simulations (line).

residence time (at the expense of the synchronization efficiency). Thus far, SR and RA are typically treated separately in the literature. This is due to the fact that SR is usually examined as a function of the *noise intensity*, while RA is studied as a function of the characteristic time scales which reign over the barrier modulation process, such as the correlation time scale of the applied nonequilibrium noise [8–11]. It should also not go unnoticed that the strict coherent external driving implies that SR results from a *non-stationary* process while typically the use of a stationary noise that is employed for RA causes a time-homogeneous escape dynamics, possessing a stationary mean residence time [8–11]. Moreover, in SR the average rate of escape for *weak* driving strengths typically decays monotonically, with respect to both increasing driving frequency and increasing noise strength [15]. This result, however, may no longer hold true in the regime of nonlinear response [16]. It is this situation, with our system being driven at strong, but still subthreshold strengths which we shall address with this work.

Given the possibility that both phenomena can occur simultaneously, the objective of our study is to contrast SR and RA for a driven stochastic metastable dynamics. In particular, we demonstrate that RA is observed in the generic model system which is typically used to examine SR, *i.e.* a rocked, non-inertial (*i.e.* overdamped) bistable dynamics. This is achieved by a comparative experimental and numerical investigation of the behavior of a heavily damped particle in a periodically modulated bistable potential for different modulation frequencies. Experimentally, the situation is realized with a colloidal particle which is subjected to a time-dependent optical potential. The numerical study is performed by computer simulations of the Langevin dynamics of a Brownian particle moving in a corresponding potential. Despite the fact that SR and RA are observed in the same system, the conditions for both effects to occur are distinct. Consequently, these effects are observed in different regions of parameter space.

Our experimental setup consisting of scanned laser tweezers, a sample cell containing a colloidal suspension, and a video microscope was described in [6, 17]. For the measurements presented here we used silica beads of diameter $2r = 1.57\,\mu$m. Figure 1A shows the two-dimensional probability distribution $P(x, y)$ of a particle fluctuating in a (static) double-well potential created by two focussed laser spots. From the hopping process between the two wells we determined the system Kramers time of $T_{\rm K} \approx 27\,$s. The symbols in fig. 1B present a cross-section at $y \approx 0\,\mu$m of the potential determined from $P(x, y)$ using the Boltzmann distribution. From the experimentally imposed potential we can estimate the following parameters: $2x_0 = 1.8\,\mu$m, $\Delta V = 3\,k_{\rm B}T$, $A_{\rm pot} = 8k_{\rm B}T$. These will be used below for our numerical simulations. Herein, $2x_0$ denotes the separation of the static potential's minima, ΔV is the barrier height for the static potential and $A_{\rm pot}$ the potential difference between the two minima in the maximally

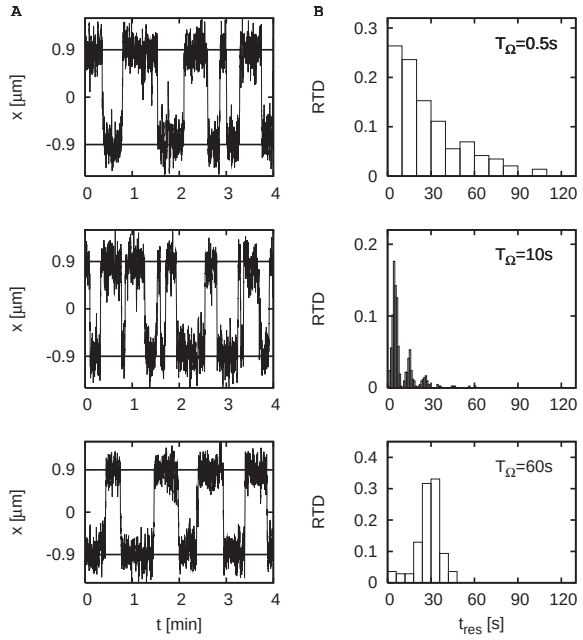

Fig. 2 – A) Sample experimental measurements of $x(t)$ for $T_\Omega = 0.5\,\mathrm{s}$, $10\,\mathrm{s}$, $60\,\mathrm{s}$. B) Corresponding histograms for the measured residence time distributions (RTD). The system is strongly driven around 85% of the threshold driving strength (as defined below eq. (3)).

tilted state of the modulated potential. Moreover, k_B denotes the Boltzmann constant and T is the temperature (room temperature in our case). The solid line in fig. 1B corresponds to the function

$$V(x) = \Delta V \left[\left(\frac{x}{x_0} \right)^2 - 1 \right]^2 \tag{1}$$

which represents the static part of the double-well potential in the simulations. In the central region which is relevant for the particle dynamics the experimental potential is described very well by this function.

The basis for the analysis of our experimental data are the particle trajectories exhibiting a bistable hopping dynamics. Figure 2A depicts typical sections of the trajectories for the modulation times $T_\Omega = 0.5\,\mathrm{s}$, $10\,\mathrm{s}$ and $60\,\mathrm{s}$, where the two potential wells were modulated sinusoidally and in opposite phase, at approximately 85% of the threshold driving strength. Here, it becomes already obvious that the mean time between particle jumps is larger both for $T_\Omega = 0.5\,\mathrm{s}$ and $60\,\mathrm{s}$ than for $T_\Omega = 10\,\mathrm{s}$ while the jumps occur most regularly for $T_\Omega = 60\,\mathrm{s}$. From these trajectories we determined the residence time distributions by applying thresholds in order to allocate the continuous particle position to either the left or the right potential well [1]. The threshold values were chosen as the positions $\pm x_0$ of the minima of the static double-well potential. Figure 2B depicts the residence time distributions for $T_\Omega = 0.5\,\mathrm{s}$, $10\,\mathrm{s}$ and $60\,\mathrm{s}$. In case of a fast modulation, *i.e.* $T_\Omega = 0.5\,\mathrm{s}$, the particle experiences *de facto* an average double-well potential. The residence time distribution thus depicts no structure and decays exponentially. For $T_\Omega = 10\,\mathrm{s}$ the particle responds to the potential modulation which results in a corresponding modulation of the transition probability. Escape events occur now more fre-

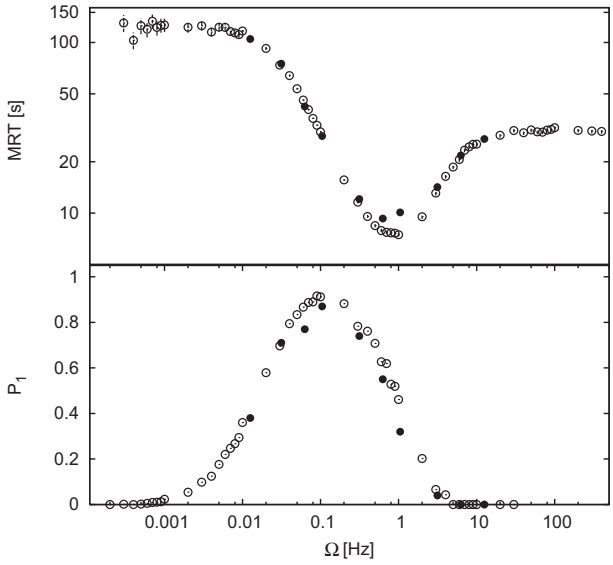

Fig. 3 – Mean residence time MRT (upper panel) and the area P_1 under the first peak of the residence time distributions (lower panel) as a function of the driving angular frequency Ω for experimental (•) and numerical (○) results.

quently as compared to $T_\Omega = 0.5\,\mathrm{s}$ and the residence time distribution displays a series of peaks which are located at odd multiples of $T_\Omega/2$, in accordance with theory [1]. This peak structure emerges naturally if we consider that a particle jumps most likely when the relevant potential barrier assumes a minimum. Then, the new relevant potential barrier assumes its minimum half a period later. So the preferred residence time is $t_{\mathrm{res}} = T_\Omega/2$. If the particle misses a "good opportunity" to jump it has to wait for another (or multiple) T_Ω. Finally, for $T_\Omega = 60\,\mathrm{s}$ the particle jumps occur very regularly. In this case the condition for stochastic resonance, $T_\Omega \approx 2T_{\mathrm{K}}$, is approximately fulfilled and we observe just a single peak in the residence time distribution.

In order to characterize resonant activation in our system we computed the mean residence time (MRT), *i.e.* the mean time the system dwells on one of the (symmetric) metastable states, as a function of the modulation parameter T_Ω. The resulting experimental values of the MRT *vs.* the angular driving frequency Ω are depicted in the upper part of fig. 3 (full symbols). The curve displays a pronounced minimum around $\Omega = 1\,\mathrm{Hz}$. For $\Omega \gg \Omega_{\mathrm{K}}$ ($\Omega_{\mathrm{K}} = 2\pi/T_{\mathrm{K}}$) the particle experiences a quasi-static potential with a time-averaged barrier height. With decreasing frequency, the particle jumps preferentially when the barrier is smallest which reduces the MRT by more than a factor of 2. For $\Omega \ll \Omega_{\mathrm{K}}$ we reach the adiabatic case where the MRT is given as the average of the mean residence times for all instantaneous potentials.

In order to compare the findings for the MRT with SR we need a measure that as well depends on the time-scale of the driving, *i.e.* the period T_Ω. Knowingly, the signal-to-noise ratio is in leading order independent of the driving period and, moreover, the spectral amplification measure [18] typically does not depict a pronounced resonance-like, bell-shaped behavior *vs.* frequency at a fixed noise strength [1,18]. A more suitable quantifier for SR that does sensitively account for the intrinsic synchronization feature of SR is the area P_1 under the first peak of the residence time distribution [19–21]. It typically exhibits a "bona-fide"-

resonance-like behavior and it is computed here according to

$$P_1 = \int_{0.3T_\Omega}^{0.7T_\Omega} P(t_{\rm res}) \mathrm{d}t_{\rm res} \ , \tag{2}$$

where $P(t_{\rm res})$ is the (normalized) residence time distribution. Within this regime of integration and our choice of driving parameters, the role of the background can safely be neglected (see fig. 2B). A preferred measure for synchronization would be the probability $P(2)$ of finding precisely 2 transitions of forward-and-backward escapes (or vice versa) per external driving period [21]. Due to a lack of stability of the modulation frequency of $\pm 10\%$ in our performed experimental time-series we cannot determine this quantifier faithfully. However, using numerical simulations we confirmed that in our case $P(2)$ depicts a peak at the same modulation frequency Ω where also P_1 shows a peak.

Our results for P_1 are depicted in the lower part of fig. 3 (full symbols). Note that the angular driving frequencies where RA and SR occur are not identical. This becomes clear when we compare the residence time distributions in fig. 2. The best synchronization between the modulation signal and the particle motion is achieved for $T_\Omega = 60\,s$. However, although the particle motion is less regular at $T_\Omega = 10\,\mathrm{s}$ and the hopping events are distributed over many peaks in the residence time distribution, the absolute timescale between jumps is shorter in this case.

In addition to our *in situ* experiments, we also performed Langevin simulations to study the motion of an overdamped Brownian particle in a double-well potential. For the sake of simplicity, we only considered a one-dimensional potential which has been demonstrated to describe our experimental situation very well [17].

The time evolution of a particle moving in a double-well potential subjected to an external periodic driving can be described in terms of the Langevin equation

$$\eta \frac{\mathrm{d}x(t)}{\mathrm{d}t} = -V'(x) + A_0 \cos(\Omega t + \phi) + \xi(t). \tag{3}$$

$x(t)$ represents the particle's position, $\xi(t)$ is a Gaussian white process with zero mean and autocorrelation $\langle \xi(t)\xi(s)\rangle = 2\eta k_{\rm B} T \delta(t-s)$, *i.e.* the Gaussian white noise arising from the heat bath, and $V(x)$ denotes the generic double-well potential defined in eq. (1). The external periodic driving is introduced by the $A_0 \cos(\Omega t + \phi) = A_0 \cos(\frac{2\pi}{T_\Omega} t + \phi)$ term, in which Ω represents the angular driving frequency, ϕ denotes the phase shift. $A_0 = A_{\rm pot}/2x_0 = (\sqrt{3}/2) A_{\rm threshold}$ is the strength of the subthreshold driving force used in the experiments. Furthermore, η denotes the friction coefficient.

Equation (3) was integrated by standard techniques of integration of stochastic differential equation with respect to the Brownian motion [22]. Properties of the system were examined by use of Monte Carlo techniques [23]. From the simulated ensemble of very long realizations of the underlying asymptotic, nonstationary stochastic process in eq. (3) the residence time distributions were evaluated and analyzed for various angular driving frequencies Ω.

The parameters of the potential and the modulation were adjusted in order to match the experimental ones as discussed above. The friction coefficient η was estimated from Stokes' formula and then adjusted numerically in order to optimally fit the agreement between experiment and simulation for the MRT. For all simulations presented here we used $\eta = 1.7 \times 10^{-8}\,\mathrm{kg\,s^{-1}}$ which is slightly higher than the value estimated from Stokes' formula [17].

As a characteristic quantifier of RA we have used up to here the MRT, as determined from the long-time trajectories. We found very good agreement with our experimental results depicted in fig. 3 (upper panel). The open symbols in fig. 3 depict the simulation results. The error bars presented in the figure have been calculated using the bootstrap method [23].

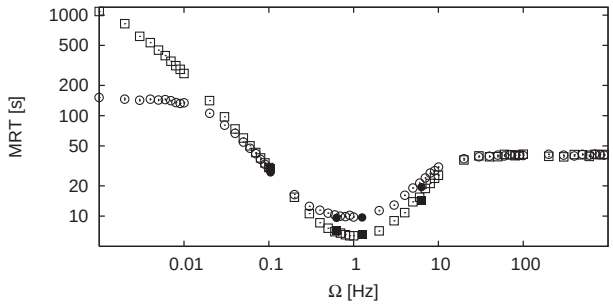

Fig. 4 – Mean residence time MRT as a function of the driving angular frequency Ω for sinusoidal (• and ∘) and square-wave driving (■ and □). Filled symbols represent the experimental findings, open squares denote the numerical simulation results.

We would like to remark here that the concept of the MRT can be readily determined from the corresponding stationary time-series of residence times of the simulations (after the transients have quieted down). In contrast, for a time-dependent, nonstationary process the concept of the mean first-passage time (MFPT) is not simply related to the MRT; this is so, because the MFPT now depends (apart from the initial condition) also on the initial time point (phase) of the forcing [24] with its mean value determined over a phase-dependent, oscillating time-inhomogeneous first-passage time density.

Finally, we also investigated how the shape of the modulation signal affects the MRT. It has already been demonstrated previously by numerical simulations that the MRT can vary significantly, depending on the shape of the modulation signal [25]. Using not the identical but similar parameters for the potential and its modulation as above, we performed a series of experiments in order to compare the MRT obtained for a sinusoidal signal (• in fig. 4) with the MRT for rectangular, square-wave driving (■ in fig. 4). In the latter case the minimum of the MRT is deeper and slightly shifted to smaller frequencies. Around $\Omega \approx \Omega_{\mathrm{K}}$ the particle jumps occur mainly when the potential barrier is smallest. Since in case of rectangular driving a small barrier is maintained over a longer time than for sinusoidal modulation with the same frequency, this leads to a deeper minimum in the MRT curve. In the adiabatic limit, *i.e.* at $\Omega \ll \Omega_{\mathrm{K}}$, the sinusoidal driving yields a smaller MRT because the average of the mean residence times for all instantaneous potentials is smaller than for rectangular driving. For $\Omega \gg \Omega_{\mathrm{K}}$ the particle experiences an average potential and the MRT is independent of the shape of the driving signal. The open symbols in fig. 4 correspond to Langevin simulation results which show excellent agreement with the corresponding experimental data (filled symbols).

Conclusion. – Experimental and numerical studies evidence that stochastic resonance and resonant activation can be observed in the very same system of an overdamped Brownian dynamics that stochastically evolves in a periodically modulated double-well potential. We have explicitly addressed the correlation between the two effects which despite certain similarities probe rather different properties of the system dynamics. The detection of SR indicates the high level of synchronization of the particle position with the external periodic driving while the presence of RA indicates an optimal speed-up of the kinetics (*i.e.* the inverse of the MRT) of the barrier crossing process. We demonstrated that with a strong sub-threshold driving a single parameter (in our case the modulation frequency) is sufficient to optimize the system either for SR or for RA. Yet another class of related systems that comes to mind where this beneficial interplay between RA and SR crucially determines the physics are rocked Brownian motor devices which are able to perform work against external bias forces [26].

The experimental work was supported by the DFG (BE 1788/4-1). BD acknowledges the support from the Polish State Committee for Scientific Research (KBN) grant 2P03B08225 (2003-2006) and from the Foundation for Polish Science. Computer simulations have been performed at the Academic Computer Centre CYFRONET AGH (Kraków, Poland).

REFERENCES

[1] Gammaitoni L., Hänggi P., Jung P. and Marchesoni F., *Rev. Mod. Phys.*, **70** (1998) 223.
[2] Fauve S. and Heslot F., *Phys. Lett. A*, **97** (1983) 5.
[3] McNamara B., Wiesenfeld K. and Roy R., *Phys. Rev. Lett.*, **60** (1988) 2626.
[4] Giacomelli G., Marin F. and Rabbiosi I., *Phys. Rev. Lett.*, **82** (1999) 675.
[5] Simon A. and Libchaber A., *Phys. Rev. Lett.*, **68** (1992) 3375.
[6] Babič D., Schmitt C., Poberaj I. and Bechinger C., *Europhys. Lett.*, **67** (2004) 158.
[7] Hänggi P., *ChemPhysChem*, **3** (2002) 285.
[8] Doering C. R. and Gadoua J. C., *Phys. Rev. Lett.*, **69** (1992) 2318.
[9] Pechukas P. and Hänggi P., *Phys. Rev. Lett.*, **73** (1994) 2772.
[10] Reimann P. and Hänggi P., *Lect. Notes Phys.*, **484** (1997) 127.
[11] Reimann P., Bartussek R. and Hänggi P., *Chem. Phys.*, **235** (1998) 11.
[12] Mantegna R. N. and Spagnolo B., *Phys. Rev. Lett.*, **84** (2000) 3025.
[13] Dybiec B. and Gudowska-Nowak E., *Fluct. Noise Lett.*, **4** (2004) L273.
[14] Juraszek J., Dybiec B. and Gudowska-Nowak E., *Fluct. Noise Lett.*, **5** (2005) L259;
[15] Jung P., *Z. Phys. B*, **76** (1989) 521; cf. figs. 5 and 6 therein for $A = 0.1$.
[16] Casado-Pascual J. *et al.*, *Phys. Rev. Lett.*, **91** (2003) 210601; Casado-Pascual J. *et al.*, *Europhys. Lett.*, **58** (2002) 342.
[17] Evstigneev M. *et al.*, *J. Phys.: Condens. Matter*, **17** (2005) S3795.
[18] Hänggi P. and Jung P., *Europhys. Lett.*, **8** (1989) 505; Hänggi P. and Jung P., *Phys. Rev. A*, **44** (1991) 8032.
[19] Gammaitoni L., Marchesoni F. and Santucci S., *Phys. Rev. Lett.*, **74** (1995) 1052.
[20] Park K. and Lai Y. C., *Europhys. Lett.*, **70** (2005) 432.
[21] Talkner P. *et al.*, *New J. Phys.*, **7** (2005) 14.
[22] Higham D. J., *SIAM Rev.*, **43** (2001) 525.
[23] Newman M. E. J. and Barkema G. T., *Monte Carlo Methods in Statistical Physics* (Clarendon Press, Oxford) 1999.
[24] Schindler M., Talkner P. and Hänggi P., *Phys. Rev. Lett.*, **93** (2004) 048102; *Physica A*, **351** (2005) 40.
[25] Zolotaryuk Y., Ermakov V. N. and Christiansen P. L., *J. Phys. A*, **37** (2004) 6043.
[26] Astumian R. D. and Hänggi P., *Phys. Today*, **55**, No. 11 (2002) 33; Linke H., *Appl. Phys. A*, **75** (2002) 167 (special issue); Reimann P. and Hänggi P., *Appl. Phys. A*, **75** (2002) 169; Babič D., Schmitt C. and Bechinger C., *Chaos*, **15** (2005) 026114; Hänggi P., Marchesoni F. and Nori F., *Ann. Phys. (Berlin)*, **14** (2005) 51.